Pergamon

Geochimica et Cosmochimica Acta, Vol. 67, No. 20, pp. 3817–3832, 2003

0016-7037/03 $30.00 + .00

doi:10.1016/S0016-7037(00)00176-5

Mechanism, rates, and consequences of basaltic glass dissolution: II. An experimental study of the dissolution rates of basaltic glass as a function of pH and temperature

SIGURDUR R. GISLASON[1,*] and ERIC H. OELKERS[2]

[1]Science Institute, University of Iceland, Dunhagi 3, 107 Reykjavik, Iceland
[2]Géochimie, Transferts et Mécanismes, CNRS/URM 5563-Université Paul Sabatier, 38 rue des Trente-six Ponts, 31400 Toulouse, France

(*Received November* 29, 2001; *accepted in revised form February* 18, 2003)

Abstract—This study is aimed at quantifying surface reaction controlled basaltic glass dissolution rates at far-from-equilibrium conditions. Towards this aim, steady-state basaltic glass dissolution rates were measured as a function of pH from 2 to 11 at temperatures from 6° to 50°C, and at near neutral conditions to 150°C. All rates were measured in open system titanium mixed flow reactors. Measured dissolution rates display a common pH variation; dissolution rates decrease dramatically with increasing pH at acid conditions, minimize at near neutral pH, and increase more slowly with increasing pH at basic conditions. The pH at which basaltic glass dissolution minimizes decreases with increasing temperature.

Dissolution rates were interpreted within the context of a multioxide dissolution model. Constant temperature rates are shown to be consistent with their control by partially detached Si tetrehedra at the basaltic glass surface. Regression of far-from-equilibrium dissolution rates obtained in the present study and reported in the literature indicate that all data over the temperature and pH range $6° < T < 300°C$ and $1 < pH < 11$ can be described within uncertainty using

$$r_{+,geo} = A_A \exp^{-(E_A/RT)} \left(\frac{a^3_{H^+}}{a_{Al^{3+}}} \right)^{1/3}$$

where $r_{+,geo}$ signifies the geometric surface area normalized steady-state basaltic glass dissolution rate at far-from-equilibrium conditions, A_A refers to a constant equal to $10^{-5.6}$ (mol of Si)/cm^2/s, E_A, designates *a pH independent activation energy* equal to 25.5 kJ/mol, R stands for the gas constant, T signifies temperature in K, and a_i represents the activity of the subscripted aqueous species.

1. INTRODUCTION

Chemical weathering of Ca, Mg-silicates on land and the ocean floor governs the long term atmospheric CO_2 content, and chemical weathering influences strongly the composition of soil waters, rivers, and the oceans (Urey, 1952; Riley and Chester, 1971; Holland, 1978; Thompson, 1983; Berner, 1992; Spivack and Staudigel, 1994; Brady and Gislason, 1997; Chester, 2000; Kump et al., 2000). Because of its abundance at the Earth's surface and its high reactivity, chemical weathering of both glassy and crystalline basalt plays a significant role in the global cycle of numerous elements (Gislason et al., 1996; Brady and Gislason, 1997; Louvat, 1997; Moulton et al., 2000; Dessert et al., 2001; Stefánsson and Gislason, 2001). Low temperature alteration by seawater of Ca-bearing silicates in basalt and of basatic glass is estimated to release as much Ca to the world's oceans as continental weathering (McDuff and Morel, 1980; Alt et al., 1986; Staudigel et al., 1989; Francois and Walker, 1992; Spivack and Staudigel, 1994; Berner and Berner, 1996; Brady and Gislason, 1997).

Chemical weathering is a complex process involving coupling and feedback of dissolution, precipitation, and mineral replacement reactions, which can involve stress-mediated coupling between crystal growth and pressure solution of neighboring crystals where volume is preserved (i.e., Wang et al., 1995). Of these processes, the present study focuses on the rates of basaltic glass dissolution, a process that is particularly significant during the early stages of basalt weathering. Humpris and Thompson (1978), Kristmannsdóttir and Tómasson (1978), Kristmannsdóttir (1982), Colman (1982), Eggleton et al. (1987), Banfield et al. (1991), and Nesbitt and Wilson (1992) observed, that basaltic and interstitial rhyolitic glass, and olivine are the first phases altered during terrestrial or oceanic seafloor weathering. Although the rapid weathering of natural glass has been attributed to the faster dissolution rate and higher solubility of the glasses relative to the crystals (Gislason and Eugster, 1987; Gislason and Arnórsson, 1990, 1993; Gislason et al., 1996), basaltic glass weathering may also be enhanced by a relatively high surface area or its better access to undersaturated aqueous solutions. For example, the tops and bottoms of terrestrial and sub oceanic lava flows are glazed with basaltic glass, whereas their interiors are comprised of crystalline basalt. The same applies to pillow lavas formed on the ocean floor; the core of the pillows is crystalline but their surfaces glassy. The hydraulic conductivity of the basaltic lava flows and pillow lavas is always greatest along the glassy part of the flows (Sigurdsson and Ingimarsson, 1990) further enhancing the weathering rate of the glass relative to the crystalline interior. Basaltic glass dissolution will, therefore, tend to dominate the early weathering stages of oceanic crust and terrestrial basalt.

Despite its role in chemical weathering, there are very few dissolution rate data available for basaltic glass at the low temperatures and pH typical of many Earth surface processes.

* Author to whom correspondence should be addressed (sigrg@raunvis.hi.is).

Chemical weathering on land and the ocean floor takes place at temperatures from 0° to ~30°C and pH 2 to 11 (Gislason et al., 1992, 1996; Chester, 2000). With the exception of Crovisier's (1989) work, all basaltic glass dissolution rate determinations have been performed at the temperatures of 25°C or higher. Existing experimental studies of weathering and/or alteration of basalt and basaltic glass have focused on the variation of rates with temperature, pH, water composition, glass content, basalt-seawater ratio, and the presence of bacteria (Hoppe, 1940; Furnes, 1975; Seyfried and Bischoff, 1979; Crovisier et al., 1985, Berger et al., 1987, 1988, 1994b; Gislason and Eugster, 1987; Crovisier, 1989; 1987; Guy, 1989; Guy and Schott, 1989; Thomassin et al., 1989; Gislason et al., 1993; Teng and Grandstaff, 1995; Thorseth et al., 1995; Brady and Gislason, 1997; Daux et al., 1997; Oelkers et al., 1999; Oelkers and Gislason, 2001).

The overall goal of this manuscript series is to 1) determine the mechanism and develop predictive equations describing both long and short term basaltic glass dissolution rates as a function of temperature and solution composition including pH, organic acid concentration, and basaltic glass saturation state, and 2) apply these equations to the improved understanding of the extent and consequences of basaltic glass dissolution in natural systems. In the first paper in this series (Oelkers and Gislason, 2001), steady-state basaltic glass dissolution rates were measured as a function of aqueous Si, Al, and organic acid concentration at 25°C and the pH of 3 and 11. These data were used to establish the basaltic glass dissolution mechanism, and to generate a transition state theory based 'far-from-equilibrium' rate equation. This second manuscript is aimed at quantifying basaltic glass dissolution rates as a function of pH and temperature. Towards this goal far-from-equilibrium basaltic glass dissolution rates were measured over a broad pH range at temperatures from 6 to 150°C. These results were used together with rates obtained from the literature to generate a consistent set of equations describing steady-state far-from-equilibrium basaltic glass dissolution rates as a function of pH and solution composition from 0 to 300°C. The purpose of this paper is to describe the results of this combined experimental and theoretical study.

2. THEORETICAL BACKGROUND

The standard state adopted in this study is that of unit activity for pure minerals and H_2O at any temperature and pressure. For aqueous species other than H_2O, the standard state is unit activity of the species in a hypothetical 1 molal solution referenced to infinite dilution at any temperature and pressure. All aqueous activities and chemical affinities in the present study were generated using EQ3NR (Wolery, 1983). Equilibrium constants used in these calculations were taken from SUPCRT92 (Johnson et al., 1992) for all species and minerals other than 1) aqueous Al-bearing complexes, which were taken from Pokrovskii and Helgeson (1995), and 2) hydrated basaltic glass. The only significant Al-bearing aqueous species considered in the thermodynamic model are Al^{3+}, $Al(OH)^{2+}$, $Al(OH)_2{}^{+}$, $Al(OH)_3{}^{0}$, and $Al(OH)_4{}^{-}$. The equilibrium constant for hydrated basaltic glass hydrolysis, consistent with the reaction

$$SiAl_{0.36}O_2(OH)_{1.08} + 1.08\ H^+ = SiO_{2(aq)} + 0.36\ Al^{3+} + 1.08\ H_2O, \quad (1)$$

was estimated from the stoichiometrically weighted sum of the amorphous silica and gibbsite hydrolysis reactions (see Bourcier et al., 1989; Daux et al., 1997). Values of the logarithm of the equilibrium constant of reaction 1 were generated using the SUPCRT92 computer code. Resulting values were 0.261, 0.027, −0.693, and −1.105 at 0°, 30°, 100°, and 150°C, respectively.

The overall dissolution rate of a mineral or glass may be influenced by numerous factors including 1) the aqueous transport of chemical species away from its surface (cf. Murphy et al., 1989), 2) the effect of inverse reaction at near to equilibrium conditions (cf. Oelkers et al., 1994), and 3) the far-from-equilibrium dissolution rate. The goal of this current study is to quantify far-from-equilibrium basaltic glass dissolution exhibiting surface reaction control. All rates measured and retrieved from the literature in the present study correspond, therefore, to surface reaction controlled far-from-equilibrium steady-state basaltic glass dissolution rates.

One challenge in quantifying mineral or glass dissolution rates is that there are two different distinct surface reactions that can lead to rate variation with solution composition: 1) the inverse reaction, or the tendency to reprecipitate a solid as equilibrium is approached, and 2) the reaction forming the rate controlling activated or precursor complex. The first of these effects is often quantified in terms of the chemical affinity of the dissolving phase leading to an equation of the form (Aagaard and Helgeson, 1977, 1982; Lasaga, 1981; Helgeson et al., 1984; Murphy and Helgeson, 1987; Oelkers, 2001)

$$r = r_+(1 - \exp(-A^* / \sigma RT)), \quad (2)$$

where r and r_+ designate the overall and forward dissolution rate, respectively, A^* refers to the chemical affinity for the solid surface layer hydrolysis reaction, which may differ from that of the bulk solid, σ stands for Temkin's average stoichiometric number equal to the ratio of the rate of destruction of the activated or precursor complex relative to the overall rate, R designates the gas constant, and T represents absolute temperature. Numerous studies have adopted a form of Eqn. 2 to describe the variation of basaltic glass dissolution on solution composition at near to equilibrium conditions. For example, Grambow (1985) and Berger et al. (1994b) observed that the solid surface layer during glass dissolution consists of an amorphous Si-rich layer and suggested that A^* can be assumed equal to the chemical affinity of amorphous silica. In contrast, Bourcier et al. (1989) and Daux et al. (1997) suggested that A^* can be assumed equal to the chemical affinity of an amorphous gel containing $SiO_2 + Al(OH)_3 \pm Fe(OH)_3$, $Ca(OH)_2$ and $Mg(OH)_2$. Each of these studies accurately described various glass dissolution data sets as a function of solution composition at near to equilibrium conditions.

In contrast to these previous studies, the present study is focused on basaltic glass dissolution rates at far-from-equilibrium conditions. This allows determination of the effect on rates of the activated or precursor complex formation reaction independently of those stemming from the inverse reaction. The form of Eqn. 2 is such that overall rates (r) equal forward

rates (r_+) when $A^* \gg \sigma RT$. As one approaches equilibrium, overall rates (r) decrease systematically and are equal to zero at equilibrium with the surface, where $A^* = 0$. According to Eqn. 2, r is within 10% of r_+ when $A^*/\sigma RT > 2.3$. All dissolution rates measured in the present study were performed at conditions where $A^*/RT > 5$, where in this case A^* refers to the chemical affinity of hydrated basaltic glass in accord with reaction 1.

The variation with solution composition of r_+, the forward or far-from-equilibrium dissolution rate, can be deduced from the dissolution mechanism. In accord with Oelkers and Gislason (2001), basaltic glass dissolution is assumed to consist of a series of metal for proton exchange reactions at the glass surface of the form:

$$>M + nH^+ = >H_n + M^{+n} \quad (3)$$

where $>M$ refers to the metal M in the glass near surface structure and $>H_n$ represents n protons present in this metal site. Reaction 3 is written such that the number of protons added to the glass structure balances the charge removed by the metal M^{+n}. Evidence supporting this assumption for a variety of minerals and glasses is summarized by Oelkers (2001). Reaction 3 proceeds via the breaking of metal-oxygen bonds and their replacement with proton oxygen bonds in the glass near surface structure. Differences in the rates of breaking different types of metal-oxygen bond within the glass near surface structure is sufficiently large that after a short time all of the metal-proton exchange reactions attain equilibrium with the fluid other than that involving the slowest breaking bond necessary to hold together the glass structure. For the case of basaltic glass, these slowest breaking bonds are tetrahedral Si-O bonds. The equilibrium constants of exchange reactions involving monovalent and divalent cations, which are commonly viewed as being loosely bound to the glass structure, are sufficiently large such that these metals are essentially completely removed from the basaltic glass near surface. In contrast, equilibrium constants for those exchange reactions involving trivalent cations, which are generally viewed as being strongly bound, are relatively small such that only a small fraction of these cations are removed via proton exchange reactions.

The final step is the destruction of tetrahedrally coordinated Si-O bonds, which are the slowest breaking bonds necessary for maintaining the basaltic glass framework. Si tetrahedra on the basaltic glass surface may be connected to the basaltic glass framework via one, two, or three bridging oxygens; the rate of liberating any Si atom at the basaltic glass surface decreases dramatically as the number of bridging oxygen bonds increases (cf. Gratz et al., 1991; Gratz and Bird, 1993; Gautier et al., 2001). Any Si atom at the basaltic glass surface bound by only a single bridging oxygen is rapidly liberated; all but newly ground surfaces will be essentially free of Si atoms bound by a single bridging oxygen, and will contain only Si atoms bound by two or three bridging oxygens. It seems likely, therefore, that the overall rate of breaking the hydrated basaltic glass will be controlled by the concentration of Si atoms bridged by two bridging oxygens (Si^{II}) at the basaltic glass surface (see Oelkers, 2001). The two major sources of Si^{II} are 1) Si atoms at glass edges and 2) Si atoms adjoining previously exchanged trivalent metals; the exchange of aluminum for three protons at the surface leads to the formation of three partially liberated Si^{II} atoms in accord with

$$Al\left(\begin{array}{c} O- \\ -O-Si \leftarrow O-Si- \\ O-Si- \end{array}\right)_3 + 3H^+ \rightleftarrows Al^{3+} + 3\left(\begin{array}{c} O- \\ H-O-Si \leftarrow O-Si- \\ O-Si- \end{array}\right). \quad (4)$$

On the left hand side of this reaction, the central Si atoms are linked by three bridging oxygens to the basaltic glass structure, on the right side of this reaction the central Si are linked by only two bridging oxygens to the basaltic glass structure. The non bridging oxygen, which appears as O- in reaction 4, may be bonded to nothing (and thus correspond to a $-O^-$ surface species), one or two protons, or an adsorbed cation, depending on pH and/or solution composition. It should be emphasized that exchange reaction 4 does not require aqueous protons as reactants at basic pH; at basic conditions this aluminum exchange reaction can be expressed as

$$Al\left(\begin{array}{c} O- \\ -O-Si \leftarrow O-Si- \\ O-Si- \end{array}\right)_3 + 3H_2O + OH^- \rightleftarrows Al(OH)_{4^-} + 3\left(\begin{array}{c} O- \\ H-O-Si \leftarrow O-Si- \\ O-Si- \end{array}\right). \quad (5)$$

The following derivation is based on the assumption that the number of Si^{II} atoms formed from aluminum exchange reactions is far in excess of those present at glass edges. This appears to be the case for steady-state dissolution; Si at edges tend to dissolve rapidly as demonstrated by the observation that glass grains are rounded during dissolution (see below, and Gautier et al., 2001). In contrast, Si^{II} atoms formed from aluminum exchange reactions are continuously renewed by reaction 4. Assuming basaltic glass forward dissolution rates (r_+) are proportional to the concentration of Si^{II} atoms formed from reaction 4, one can write (cf. Oelkers, 2001)

$$r_+ = ks\left(\left(\frac{a_{H^+}^3}{a_{Al^{3+}}}\right)\Big/\left(1 + K_4\left(\frac{a_{H^+}^3}{a_{Al^{3+}}}\right)\right)\right)^{1/3}, \quad (6)$$

where k refers to a rate constant, s represents the basaltic glass surface area, a_i stands for the activity of the subscripted aqueous species, and K_4 designates the equilibrium constant for reaction 4. Eqn. 6 is a general equation valid in all far-from-equilibrium solutions. The effect of the presence of aqueous inhibitors and catalysis are accounted for by their affect on aqueous Al^{3+} activity. Moreover, at extremely low aqueous aluminum activities, Eqn. 6 yields a constant rate equal to $ks(1/K_4)^{1/3}$, consistent with the concept of a 'dissolution plateau' (cf. Lasaga et al., 1994; Schott and Oelkers, 1995). In contrast, when there is a significant Al concentration at the near surface, which seems to be the case for basaltic glass at most aqueous solution compositions found in nature and in the laboratory (see below), $K_4(a_{H^+}^3/a_{Al^{3+}})$ is substantially less than 1 and Eqn. 6 reduces to

$$r_+ = ks\left(\frac{a^3_{H^+}}{a_{Al^{3+}}}\right)^{1/3}. \quad (7)$$

This approach differs from that suggested by Daux et al. (1997) who suggested, based only on rates they measured at near-to-equilibrium conditions, that basaltic glass dissolution rates are proportional to a Si-Al rich precursor with the same Si/Al ratio of the dissolving glass. In accord with their model, there would be no affect of aqueous Al on far-from-equilibrium basaltic glass dissolution rates. Daux et al. (1997) did, however, note that they could not test this possibility because they did not measure basaltic glass dissolution rates at far-from-equilibrium conditions. It has subsequently been demonstrated that far-from-equilibrium basaltic glass dissolution rates are functions of aqueous aluminum concentration at both acid and basic conditions (Oelkers and Gislason, 2001). The approach adopted in the present study also differs from that of Berger et al. (2002), who suggested that aluminosilicate dissolution could occur either by the hydrolysis of Al-O or Si-O bonds and the bulk rate equals the faster of these two hydrolysis reactions. It is unclear to what degree the Berger et al. (2002) model will apply to basaltic glass, because the destruction of all Al-O bonds will not destroy the basaltic glass structure. The destruction of the basaltic glass structure requires the breaking of at least some Si-O bonds. Moreover, there is no evidence that, as suggested by the Berger et al. (2002) model, that there is an affect of aqueous Si concentration on basaltic glass dissolution rates at far-from-equilibrium conditions.

The logarithmic analog of Eqn. 7 can be written

$$\log \frac{r_+}{s} = \log k + 1/3 \log\left(\frac{a^3_{H^+}}{a_{Al^{3+}}}\right). \quad (8)$$

Eqn. 8 suggests that constant pH far-from-equilibrium basaltic glass dissolution rates will be independent of aqueous Si activity, but decrease with aqueous Al activity (e.g., increasing aqueous Al concentration or decreasing aqueous Al complex formation). Basaltic glass dissolution rates as a function of aqueous Si, Al, and organic acid concentration at 25°C and pH 3 and 11 were found to closely correspond to those computed using Eqn. 8 (Oelkers and Gislason, 2001). Eqn. 8 will be used below to describe constant temperature basaltic glass dissolution rates as a function of aqueous solution composition.

3. SAMPLE PREPARATION AND EXPERIMENTAL METHODS

The basaltic glass used in the experiments is volcanic ash collected from the Stapafell Mountain, southwestern Iceland. The glass contains less than 1% quenched crystals. This sample is identical to that studied and described by Oelkers and Gislason (2001); its chemical composition is consistent with $Na_{0.08}Ca_{0.263}Mg_{0.281}Fe_{0.188}Al_{0.358}SiO_{3.32}$. It is close to the composition of mean oceanic crust (Ronov and Yaroshevsky, 1976) and mean ocean ridge basalt, MORB (GERM, 2000). The ash was dried, first at ambient temperature in the laboratory and then at 110°C overnight. This sample was ground then dry sieved to obtain the size fraction between 40 μm and 120 μm. It was then ultrasonically cleaned, first in deionized water, and then in acetone, by separating the ultra fine suspension at the end of each cleaning cycle, which lasted for 10 min. Four to seven water cycles and five to nine acetone cycles were adequate to remove all fine particles. Subsequently the sample was dried overnight at 110°C. The specific surface area of this material before and after the experiment was measured by the three point BET method using Kr gas with He as carrier for specific surface areas smaller than 30000 cm^2/g but N_2 gas when the surface area was greater than 20,000 cm^2/g. The precision of the measurements was ±10%. Measured surface areas are shown in Table 1. The BET surface area of the initial powder was 23000 cm^2/g, which is almost two orders of magnitude higher than its estimated geometric surface area of 250 cm^2/g (see below). Glass powders were analyzed before and after dissolution experiments using a LEO 435 VP Scanning Electron Microscope (SEM) at the University Paul Sabatier in Toulouse, France. SEM images of the glass powder before experiments are shown in Figure 1. It can be seen in this figure that the initial basaltic glass grains are free of fine particles, and appear to be smooth on a micron scale. An enlargement of this image, shown in Figure 1b, reveals a large amount of roughness on a 10–100 nm scale. This latter roughness may account, in part, for the large difference between the BET and geometric surface area of this glass powder.

Table 1. BET surface area of the basaltic glass powder before and after the experiments performed in the present study.

Basaltic glass powder	Surface area (cm^2/g Kr)	Surface area (cm^2/g N_2)
Prior to experiments	23,600	22,900
After experiment BG-1		157,200
After experiment BG-2		296,600
After experiment BG-3	14,010	
After experiment BG-4	28,240	
After experiment BG-5		290,600

All dissolution experiments were performed in a titanium mixed flow reactor system. Application of mixed flow reactors to measure mineral dissolution rates have been described in detail by Dove and Crerar (1990), Berger et al. (1994a), and Oelkers and Schott (1995, 1999). A High Precision/High Pressure Liquid Chromatography Pump provided continuous fluid flow ranging from 0.9 to 10 g/min during the experiments. The precision of the fluid flow rates was ±4%. The volume of the titanium reactor was 300 mL. The solution within the reactor was stirred by a Parr magnetically driven stirrer, the temperature controlled by a Parr controlled furnace, and elevated pressure was maintained using a back pressure regulator. Although it has been argued that stirring mixed flow reactors may lead to increasing surface areas during dissolution experiments (Metz and Ganor, 2001), this does not appear to be the case in the present study; measured surface areas of basaltic glass powders after dissolution in neutral to basic solutions are found to be similar to that of the unreacted powder (see below and Tables 1, 2, and 3). Temperature of experimental runs performed below 25°C was controlled by placing the reactor in a cooling jacket. The temperature of individual experiments ranged from 6°C to 150°C, and pressure for experiments performed in excess of 100°C was kept slightly above the liquid-vapor curve of H_2O. The fluid left the reactor through a 1 μm titanium filter, was quenched, passed through the back pressure regulator, and finally through a 0.2 μm cellulose acetate filter to the outlet, where it was sampled. For experiments performed at pH > 7, outlet solution pH was measured in a flow cell attached directly to the pressure regulator outlet to ensure that measured pH was not affected by atmospheric CO_2.

Each experimental series consisted of several different experiments performed on a single basaltic glass powder. A list of the sequence of conditions performed during each series is listed in Table 2. At the beginning of each experimental series the reactor was dismantled at ambient conditions. A specific mass of dry glass powder was placed in the reactor. The reactor was filled with the starting solution, closed, and placed in the furnace or cooling jacket. The temperature, pressure, and flow and stirring rate were adjusted to desired settings. Fluid flow rate and outlet solution composition were measured regularly. When steady-state conditions were confirmed for any experimental condition, the inlet solution composition, temperature, pressure, and/or fluid flow rate were changed to the next desired setting.

The inlet solutions used in this study were comprised of demineralized H_2O plus sufficient quantities of regent grade HCl, NH_4Cl, and/or NH_3 to obtain a 0.01 mol/kg ionic strength solution of the desired pH at 25°C. Compositions of all inlet solutions are listed in Table 3. Inlet

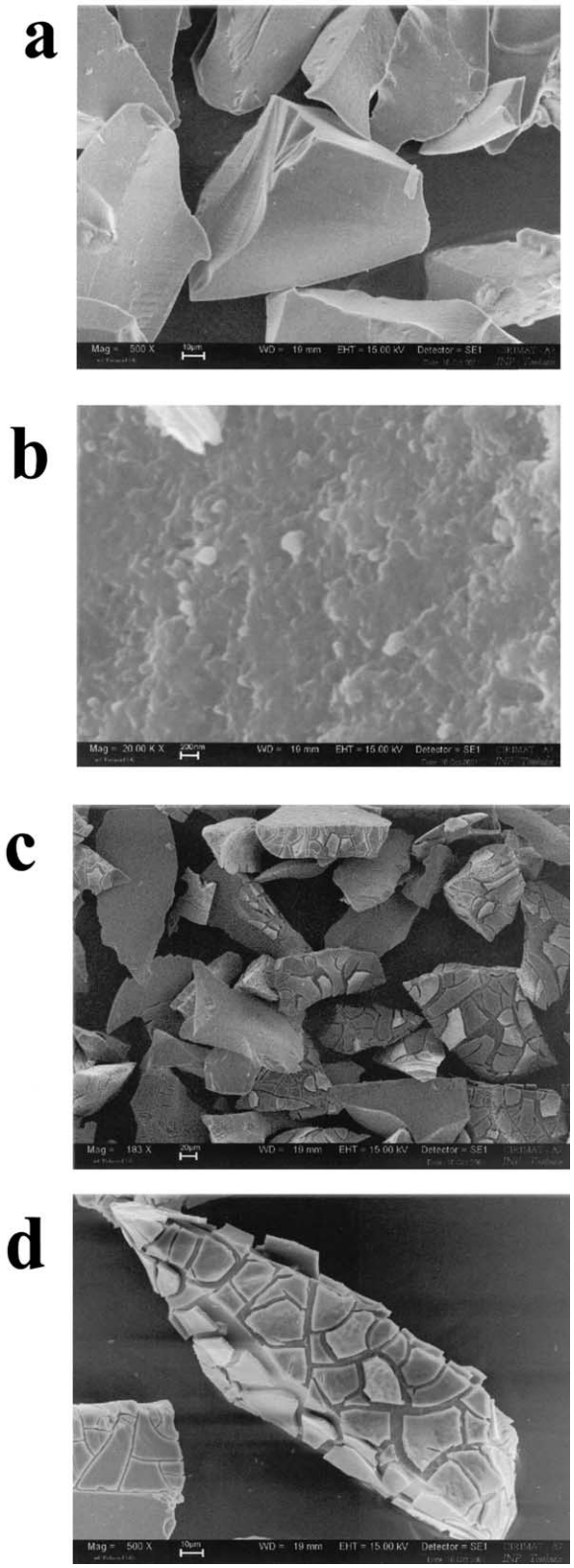

Fig. 1. Scanning electron microscope images of the basaltic glass powder used in the present study. Images (a) and (b) are of the initial glass powder before the dissolution experiments. Image (b) is an enlargement of part of image (a) showing fine scale surface roughness. Image (c) and (d) show this glass powder following its dissolution during experimental series BG-5 (see text).

Table 2. Conditions at which experimental series BG1–BG6 were performed.

Experiment	Temperature	pH at 22°C	Stirring rate (rpm)
	BG1		
BG1-9	30	4.11	100
BG1-13	30	4.11	175
BG1-19	30	3.20	175
BG1-22	30	2.09	175
BG1-27	30	2.11	250
BG1-31	30	2.30	400
	BG2		
BG2-11	30	4.17	325
BG2-16	30	3.31	325
BG2-19	30	3.33	550
BG2-21	30	3.31	700
BG2-34	30	2.34	325
BG2-37	30	2.42	550
BG2-40	30	2.40	700
	BG3		
BG3-8	29	7.00	400
BG3-11	30	8.19	400
BG3-20	30	9.13	400
BG3-23b	30	10.20	400
BG3-27	30	10.80	400
	BG4		
BG4-2	30	5.35	400
BG4-6	60	5.23	400
BG4-9	100	5.91	400
BG4-15	149	7.12	400
	BG5		
BG5-2	6	4.37	350
BG5-5	6	4.85	350
BG5-10	7	6.57	350
BG5-13	7	7.74	350
BG5-17	7	8.97	350
BG5-20	7	9.79	350
BG5-22	7	10.58	350
BG5-27	10	3.34	400
BG5-28	11	2.25	550
	BG6		
BG6-2	50	3.94	350
BG6-10	50	7.03	350
BG6-15	50	7.79	350
BG6-18	50	8.93	350
BG6-23	50	9.79	350
BG6-26	50	10.33	350
BG6-37	50	3.10	450
BG6-39	49	2.14	550

solutions having pH $>$ 7 were continuously purged by N_2 during the experiments. This was done to prevent dissolved carbonate precipitation due to CO_2 entering the reactor.

The aqueous silica concentration of all inlet and outlet solutions were measured using the molybdate blue method of Fishman and Friedman (1989) with Varyan Spectrophotometer using 1 and 5 cm flow cells. All standards and blanks were obtained using the experimental inlet solutions as diluents. The precision of the aqueous Si concentration measurements was within 3% for concentrations above 50 μg/kg Si, but close to 10% for the 50–10 μg/kg Si concentration. Si and Al concentration of selected samples were measured by High Resolution Inductively Coupled Argon Plasma Mass Spectrometer (ICP-MS) at the SGAB laboratory in Luleå, Sweden. This was done for samples when sufficient solution was available after the spectroscopic measurement. These subsamples were acidified with concentrated suprapure HNO_3 before analysis. Generally less than 10% difference was found between corresponding aqueous Si concentrations determined from the two different methods. The only exception was for 3 samples having high aqueous Fe concentration; for these solutions Si concentrations ob-

Table 3. Composition of inlet solutions used in the experiments performed in the present study.

pH (25°C)	HCl (mol/L)	NH_4Cl (mol/L)	NH_4OH (mol/L)
2.00	0.01		
3.00	0.001	0.00900	
4.00	0.0001	0.00990	
5.00	0.00001	0.00999	
6.30		0.00999	0.00001
7.30		0.00990	0.00010
8.02		0.00950	0.00050
9.03		0.00650	0.00350
9.48		0.00400	0.00600
10.05		0.00150	0.00850
10.80			0.01000

tained by colorimetry were considerably higher than those obtained from ICP-MS. This is likely due to Fe interference of spectroscopic Si measurements (Fishman and Friedman, 1989). As a consequence of the potential additional uncertainty originating from Fe interference and to be consistent with aqueous aluminum analyses, the Si analyses obtained from high resolution ICP-MS are reported below when available. For all other samples, Si analyses obtained from colorimetry are reported. The relative release rates of all major metals during a different series of basaltic glass dissolution experiments will be explored in detail in a future manuscript in this series.

4. EXPERIMENTAL RESULTS AND DISCUSSION

Surface area normalized forward dissolution rates ($r_{+,i}$) were computed from measured steady-state outlet solution aqueous Si concentration using

$$r_{+,i} = \frac{c_{Si}F}{s_i} \tag{9}$$

where c_{Si} stands for the outlet aqueous Si concentration, F represents the fluid flow rate, s_i denotes the total glass surface area present in the reactor, and the index i corresponds to the method used to define surface area. Resulting dissolution rates, together with total dissolved aluminum and silica concentrations in the outlet solution, computed solution pH at each experimental temperature, and computed chemical affinity of the outlet solution with respect to hydrated basaltic glass (A^*, see reaction 1) are listed in Table 4. pH and A^* at experimental temperatures listed in this table were computed from pH measured at 25°C together with the EQ3NR computer code (Wolery, 1983). This calculation was performed using measured aqueous Al concentrations when available; in the absence of measured values, aqueous Al concentrations were estimated from measured aqueous Si concentrations assuming stoichiometric basaltic glass dissolution. EQ3NR was also used to

Table 4. Results of steady-state dissolution rate experiments as a function of pH and T at constant ionic strength. Outlet Si concentrations listed in italic font were obtained from colorimetry, whereas those listed in roman font were obtained using high resolution ICP-MS. Outlet aluminum concentrations that are underlined are supersaturated with respect to gibbsite.

Sample	Temp. (°C)	Initial BET surface area $\times 10^5$ cm^2	Flow rate (g/min)	Outlet pH at 22°C	Computed pH at in situ T	Outlet solution concentration			Dissolution rate (mol/cm^2/s)	
						Si (mg/kg)	Al (μg/kg)	A^* (kJ/mol[a])	$r_{+,BET}$ ($\times 10^{15}$)	$r_{+,geo}$ ($\times 10^{13}$)
BG5-2	6	23.13	2.19	4.37	4.37	*0.1623*		−18.80	0.915	0.841
BG5-5	6	23.13	2.20	4.85	4.86	*0.0895*		−17.92	0.507	0.467
BG5-10	7	23.13	2.20	6.57	7.08	0.0643	4.48	−13.72	0.364	0.334
BG5-13	7	23.13	2.17	7.74	8.25	0.0799	6.42	−14.82	0.447	0.411
BG5-17	7	23.13	2.19	8.97	9.49	*0.2084*		−12.90	1.17	1.08
BG5-20	7	23.13	2.19	9.79	10.31	0.175	36.1	−15.37	0.985	0.906
BG5-22	7	23.13	2.16	10.58	11.11	0.26	60.9	−14.70	1.44	1.33
BG5-27	10	23.13	7.55	3.34	3.34	1.63	1700	−16.46	31.7	29.1
BG5-28	11	23.13	7.64	2.25	2.25	7.53	6990	−17.92	148	136
BG2-11	30	11.47	4.08	4.17	4.17	0.224	192	−18.50	4.74	4.36
BG-21	30	11.47	8.40	3.31	3.31	1.82	1610	−16.58	79.3	73.0
BG2-40	30	11.47	8.82	2.40	2.40	19.2	17400	−14.23	879	808
BG3-8	29	1.17	1.47	7.00	6.75	0.053	8.09	−18.03	3.97	3.65
BG3-11	30	1.17	3.13	8.19	7.94	0.0464	10.9	−20.27	7.39	6.80
BG3-20	30	1.17	4.56	9.13	8.88	0.0656	14.9	−21.05	15.2	14.0
BG3-23b	30	1.17	5.04	10.20	9.95	0.0646	20.2	−22.99	16.6	15.3
BG3-27	30	1.17	9.19	10.80	10.55	0.0538	16	−24.93	25.2	23.1
BG6-2	50	1.25	5.99	3.94	3.94	0.0638	27.2	−25.36	18.3	16.8
BG6-10	50	1.25	5.46	7.03	6.23	0.03	4.36	−23.34	7.83	7.20
BG6-15	50	1.25	5.77	7.79	6.99	0.0762	9.5	−21.42	21.0	19.4
BG6-18	50	1.25	6.07	8.93	8.13	0.0704	15.6	−24.33	20.4	18.8
BG6-23	50	1.25	8.16	9.79	8.99	0.0585	16.8	−25.37	22.8	21.0
BG6-26	50	1.25	9.33	10.33	9.52	0.106	31.3	−26.63	47.3	43.5
BG6-37	50	1.25	9.15	3.10	3.10	0.726	463	−26.63	317	292
BG6-39	49	1.25	9.06	2.14	2.14	*3.3080*		−22.86	1432	1318
BG4-2	30	1.11	0.88	5.35	5.31	*0.0593*		−14.60	2.78	2.56
BG4-6	60	1.11	2.04	5.23	5.03	*0.193*		−13.47	21.0	19.3
BG4-9	100	1.11	2.03	5.91	4.80	*0.638*		−13.12	69.2	63.6
BG4-15	149	1.11	2.05	7.12	4.58	*2.81*		−13.86	309	284

[a] In the absence of measured aqueous aluminum concentration data, A^* was estimated assuming stoichiometric Al/Si release.

evaluate the saturation state of the outlet solutions with respect to potential secondary phases. These calculations indicate that the outlet solutions were undersaturated with respect to silicate and aluminosilicate phases, but several solutions were supersaturated with respect to potentially precipitating aluminum oxy-hydroxide phases. Those aqueous aluminum outlet concentrations estimated to be supersaturated with respect to gibbsite are underlined in Table 4.

Rates were computed in the present study using Eqn. 9 together with glass surface areas obtained from both 1) BET gas adsorption techniques (s_{BET}) and 2) geometric surface area (s_{geo}) estimates. Resulting rates are represented by $r_{+,BET}$ and $r_{+,geo}$, respectively and are related by

$$r_+ = r_{+,BET}s_{BET} = r_{+,geo}s_{geo}. \quad (10)$$

Both $r_{+,BET}$ and $r_{+,geo}$ are provided in Table 4 to allow the results generated in the present study to be compared to the various rates reported in the literature. Values of $r_{+,BET}$ listed in Table 4 were generated using s_{BET} of the *initial* basaltic glass powder. Note that as the surface areas of basaltic glass increased substantially during experiments performed in solutions having pH$<$3.5, use of initial surface areas may lead to uncertainties (see below). To be consistent with the studies of Guy (1989) and Guy and Schott (1989), the geometric surface areas used in this calculation was generated assuming the glass powder used in this study was comprised of identical 80μm cubes, yielding a surface area of 250 cm^2/g. As the initial basaltic glass powder BET surface area was 23000 cm^2/g, $r_{+,geo}$ values generated in the present study are 92 times larger than their corresponding $r_{+,BET}$.

BET surface areas of the mineral powders measured following experimental series BG1 to BG5 are tabulated in Table 1. Measured BET surface areas increase by roughly an order of magnitude during experimental series BG1, BG2, and BG5, but changed little during experimental series BG3 and BG4. The BET surface area was not measured following experimental series BG6. As basaltic glass powder was used at several different pH and temperature conditions it is difficult to determine unambiguously which conditions lead to these differing behaviors. It may be due, however, to the powders being exposed to and dissolved in acidic solutions. The reactive solution pH of all experiments is given in Tables 2 and 4. The basaltic glass powder in experimental series BG3 and BG4 were only dissolved in neutral to basic solutions. Series BG1, BG2, BG5, and BG6 were dissolved in solutions having pH as low as 2.09. It is only those powders exposed and dissolved in acidic solutions that exhibit a large BET surface area increases during the experiments. For this reason, all experiments series were stopped following their reaction at low pH. SEM images of basaltic glass following experimental series BG5 are illustrated in Figures 1c,d. It can be seen that material has been heterogeneously removed from these surfaces leading to a substantial increase in surface roughness. Some parts of these surfaces appear to be detaching from the original surfaces. These phenomena may be due to 1) preferential dissolution along weak areas of the glass structure related to stresses incurred during cooling; 2) effects of grain drying following the experiment and/or 3) spalling of an altered layer precipitated on the surface (see Casey et al., 1989). This latter possibility could

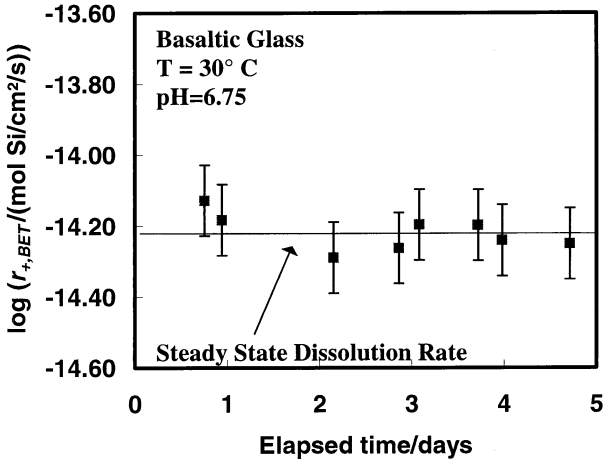

Fig. 2. Temporal evolution of measured basaltic glass dissolution rates during experiment BG3-8, which was performed at 29°C, a pH of ~7 and a fluid flow rate of 1.5 g/min. $R_{+,BET}$ values shown in this figure were obtained from aqueous Si concentrations measured using colorimetry and therefore differ slightly from that reported in Table 4 for this experiment, which are based on aqueous Si concentrations measured using high resolution ICP-MS.

stem from the pH sequence of experimental series BG1, BG2, BG5, and BG6. In each case, the experimental series was initiated at near to neutral pH, conditions where secondary precipitation of aluminum and iron oxy-hydroxides was possible. The final pH of each series was $<$ 2.5, conditions that would aggressively dissolve basaltic glass underlying any potential secondary precipitate. Due to the possibility that the increased surface area observed during experimental series BG1, BG2, BG5, and BG6 were due to effects of porous altered formation layer at the surface or sample drying following its removal from the reactor, the BET surface area of the initial powder was used to generate $r_{+,BET}$ in the present study. Nevertheless, as the potential effects of the presence of an altered layer on basaltic glass dissolution rates was not quantified in the present study, $r_{+,BET}$ measured during the end of each of these experimental series are somewhat uncertain.

A typical example of the temporal variation of dissolution rates during a single experiment is illustrated in Figure 2. This figure, which illustrates the measured rates during experiment BG3-8, was performed at 30°C, a pH of ~7 and a fluid flow rate of 1.5 gm/min. The residence time of this experiment, defined as the volume of the reactor divided by the reactive fluid flow rate, is 4 h. A fluid dynamic steady state would be attained after approximately 4 residence times if the metal release rate from the basaltic glass powder was constant. Fluid dynamic steady state may therefore be expected after this experiment proceeded 20 h. It can be seen in this figure, that all measured rates obtained after this experiment had exceeded 16 h are consistent with steady-state dissolution. To assure that all rates obtained in the present study correspond to steady-state rates, steady-state attainment of each experiment was verified using a minimum of three outlet samples taken over several residence times.

Guy (1989) and Guy and Schott (1989) noted that their measured basaltic glass dissolution rates were strongly influenced by the relatively slow diffusional transport of metals

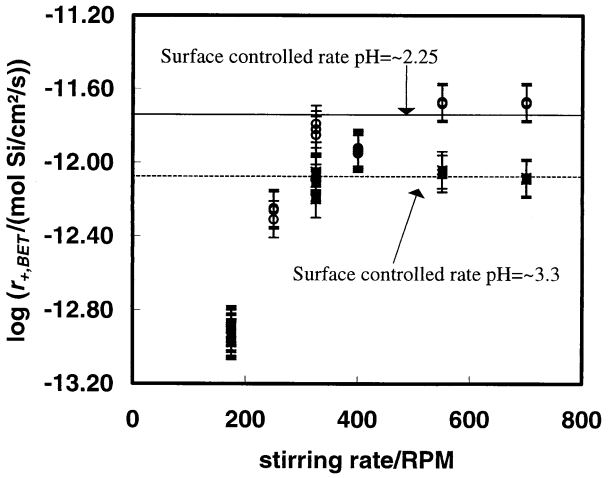

Fig. 3. Variation of measured $R_{+,BET}$ as a function of stirring rate at a temperature of 30°C. The open circles and solid squares represent data obtained at pH 2.25 ± 0.17 and 3.30 ± 0.1. Dissolution rates illustrated in this figure were obtained from experimental series BG1 and BG2. $R_{+,BET}$ values in this figure were obtained from aqueous Si concentrations measured using colorimetry and therefore differ somewhat from those reported in Table 4, which are based on aqueous Si concentrations measured using high resolution ICP-MS. The error bars correspond to a 0.1 log unit uncertainty in these rates. This uncertainty estimate is based on the fact that these dissolution rates were obtained from consecutive steady states performed on these two powders (see text).

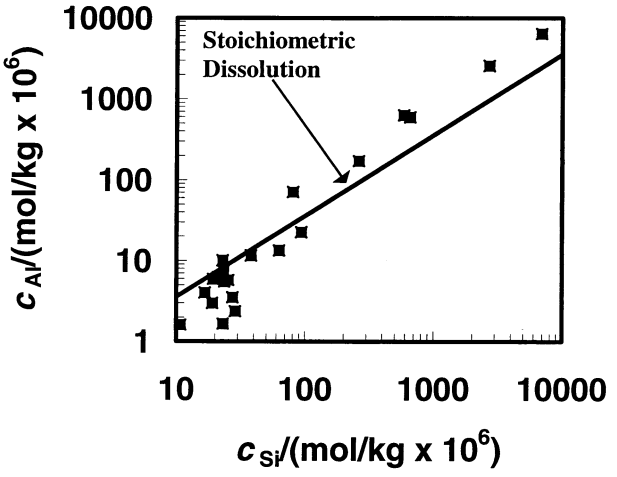

Fig. 4. The logarithm of outlet fluid Al concentration (c_{Al}) as a function of the corresponding logarithm of outlet fluid Si concentration (c_{Si}). The symbols represent measured solution compositions and the solid line corresponds to the Al/Si ratio of the dissolving basaltic glass. No error bars are shown in this figure, as the uncertainties are close to the symbol size.

from the basaltic glass surfaces at pH of less than ~2.5 and at greater than ~10. At intermediate pH, the surface release rate of metals from the basaltic glass surface was sufficiently slow such that their overall basaltic glass dissolution rate is surface reaction controlled. To assess the potential effect of slow diffusional transport on measured basaltic glass dissolution rates, several experiments were performed in the present study as a function of reactor stirring rate at acidic pH at 30°C. The results of these experiments are illustrated in Figure 3. Measured basaltic glass dissolution rates at pH 2 are independent of stirring rate above 550 rpm. At lower stirring rates, the relatively slow diffusive transport away from the basaltic glass surface results in a decrease in the overall basaltic glass dissolution rate. Measured basaltic glass dissolution rates at pH 3 are independent of stirring rate above 325 rpm. To assure, therefore, that overall basaltic glass dissolution rates listed in Table 4 are surface reaction controlled, all experiments at pH 2 and 3 were run using stirring rates greater than 550 and 400 rpm, respectively. As basaltic glass dissolution rates are slower at higher pH, measured rates, which were performed using stirring rates of 350 to 400 rpm are believed to be surface reaction controlled.

The aqueous aluminum concentration of all outlet solutions at steady state are depicted as symbols as a function of their corresponding aqueous silicon concentration in Figure 4. The solid line in this figure represents the aluminum to silicon ratio of the dissolving basaltic glass. As all inlet fluids in the present study are aluminum and silicon free, stoichiometric basaltic glass dissolution would produce outlet fluid concentrations concurrent with the line in Figure 4. It can be seen that many of the data points in the lower left side of this figure plot below the line indicating that aluminum was preferentially retained by solid phases during these experiments. This may be due to the precipitation of an aluminum oxy-hydroxide phase; several experiments exhibited outlet aqueous aluminum concentrations that were supersaturated with respect to gibbsite (see Table 4). It can also be seen that several points on the upper right side of Figure 4 plot above the line indicating that Al was preferentially released by the solids during some of the experiments. These data points correspond to outlet solution compositions measured in low pH solutions at the end of experimental series, which had previously been reacted at neutral pH/gibbsite supersaturated solutions. As such this high Al/Si outlet solution ratio may be due to the dissolution of this previously formed secondary phase. This high Al/Si outlet solution ratio may also be due to the preferential leaching of Al from the glass.

The variation of measured $r_{+,BET}$ are illustrated as a function of pH in Figure 5. These rates exhibit a pH variation common for Al-silicates; dissolution rates decrease dramatically with increasing pH at acid conditions, minimize at near neutral pH, and increase more slowly with increasing pH at basic conditions. Although data are scarce at mildly acidic conditions, the pH of minimum dissolution rate appears to decrease with increasing temperature, which is consistent with observations reported by Guy (1989) and Guy and Schott (1989). The error bars drawn in this figure were set at ±0.4 log units. The size of these error bars were chosen to reflect estimated uncertainties in the rates, as described below.

The degree to which basaltic glass dissolution rates measured in the present study are consistent with the multioxide dissolution mechanism described above and previously tested at pH 3 and 11 by Oelkers and Gislason (2001) can be assessed with the aid of Figure 6. Despite some scatter, logarithms of measured constant temperature dissolution rates appear to be a single linear function of log ($a^3_{H^+}/a_{Al^{3+}}$) at the three temperatures considered in the present study. $a_{Al^{3+}}$ values used in this figure were computed using measured aqueous Al concentrations

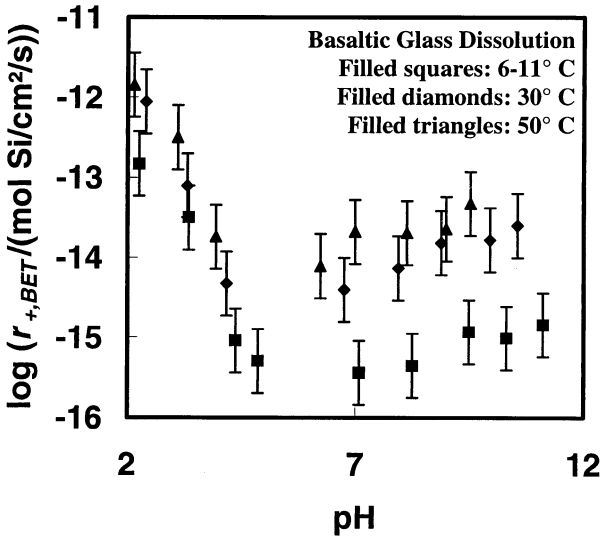

Fig. 5. Variation of measured $R_{+,BET}$ as a function of pH. The filled squares, diamonds, and triangles correspond to rates obtained at ~9°, ~30°, and ~50°C, respectively.

when available; in the absence of measured values, aqueous Al concentrations were estimated from measured aqueous Si concentrations assuming stoichiometric dissolution. The slopes of the linear regression curves shown in Figure 6 are 0.33 ± 0.18, 0.42 ± 0.12, and 0.41 ± 0.15, respectively at 6–11°, 30°, and 50°C. At each temperature, therefore, measured basaltic glass dissolution rates are consistent with Eqn. 8, and thus with the basaltic glass dissolution mechanism described above.

Comparison of rates obtained in the present study with those of Guy (1989) requires careful consideration of the different starting materials and experimental techniques adopted in this previous study. As the details of these experiments are only available in the French, a brief summary is provided. The material used in these experiments was a synthetic glass made from the rapid solidification of molten oceanic crust basalt. This glass was crushed and sieved. The 135 to 200 μm size fraction was recovered and cleaned ultrasonically. Guy (1989) estimated the surface area of this powder geometrically to be 113 cm^2/g based on the assumption that all grains were identical cubes; BET surface areas of the powders were not measured. The dissolution of this powder was performed in closed system reactors. Experiments performed at 50°C were performed in a double walled Pyrex reactor, experiments at higher temperatures were performed in 450 mL titanium reactors. The reactive fluids were comprised of 5×10^{-2} mol/L KCl plus sufficient HCl or NaOH to attain the desired pH. Seven to 10 reactive fluid samples were obtained during each closed system experiment, which lasted from several hours to 2 weeks depending on temperature and pH. Dissolution rates were determined from the temporal evolution of measured aqueous Si concentrations. Following an initial transient time, release rate of all metals other than Al and Fe were consistent with stoichiometric glass dissolution. Al release was nonstoichiometric at neutral conditions; its low concentration was attributed to gibbsite precipitation. Dissolution rates in solutions having pH of less than ~2.5 and greater than ~10 were believed to be influenced by relatively slow diffusional transport of metals from the basaltic glass surfaces; only those rates obtained in solutions having ~3<pH<~9 were believed to be surface reaction controlled.

Owing to the fact that Guy (1989) did not measure the surface areas of their powders using gas absorption techniques, unambiguous comparison of rates obtained in the present study with those of Guy (1989) can only be made using geometric surface area normalized rates. Such a comparison, of dissolution rates obtained in 50°C solutions, is presented in Figure 7. Despite the fact that these two data sets may appear to have somewhat different pH dependencies, constant pH $r_{+,geo}$ values obtained in the present study appear to be consistent, within uncertainty of those reported by Guy (1989). The close consistency between these two data sets at 50°C is noteworthy considering that the two data sets were obtained in different laboratories using significantly different experimental techniques. The observation that various basaltic glass dissolution rates are more consistent when normalized to geometric rather than BET surface area has been further confirmed by Wolff-Boenisch et al. (2002).

A single equation describing basaltic glass dissolution rates as a function of both solution composition and temperature can be generated through the application of the Arrhenius equation which is given by

$$k = A_A \exp\left(\frac{-E_A}{RT}\right) \tag{11}$$

where A_A designates a preexponential factor, E_A refers to an activation energy, R stands for the gas constant, and T signifies temperature in K. Combining this equation with Eqn. 6 yields

$$\frac{r_+}{s} = A_A \exp\left(\frac{-E_A}{RT}\right)\left(\left(\frac{a^3_{H^+}}{a_{Al^{3+}}}\right)\Big/\left(1 + K_4\left(\frac{a^3_{H^+}}{a_{Al3+}}\right)\right)\right)^{1/3} \tag{12}$$

When $K_4(a^3_{H^+}/a_{Al^{3+}})$ is substantially less than 1, which seems to be the case for basaltic glass dissolution in most natural and laboratory aqueous solutions (see below), Eqn. 12 reduces to

$$\frac{r_+}{s} = A_A \exp\left(\frac{-E_A}{RT}\right)\left(\frac{a^3_{H^+}}{a_{Al^{3+}}}\right)^{1/3} \tag{13}$$

A similar approach was used to describe successfully the dissolution rates of enstatite as a function of temperature and aqueous solution composition (Oelkers and Schott, 2001). Regression of $r_{+,geo}$ obtained in the present study, together with those reported by Guy (1989), Berger et al. (1994b), Daux et al. (1997) and Oelkers and Gislason (2001) was performed using Eqn. 13 assuming temperature and pH independent A_A and E_A. This regression yielded values of $10^{-5.6}$ (mol of Si)/cm(geo)^2/s and 25.5 kJ/mol, respectively for A_A and E_A. The degree to which these values can describe the experimentally obtained basaltic glass dissolution rates can be assessed with the aid of Figure 8 and the Appendix. The data used in this regression and listed in the Appendix were chosen for this regression because 1) these experiments were performed at far-from-equilibrium conditions, 2) aqueous aluminum concentrations of the reactive solutions were provided, and 3) experiments were performed such that measured rates were surface reaction controlled; such

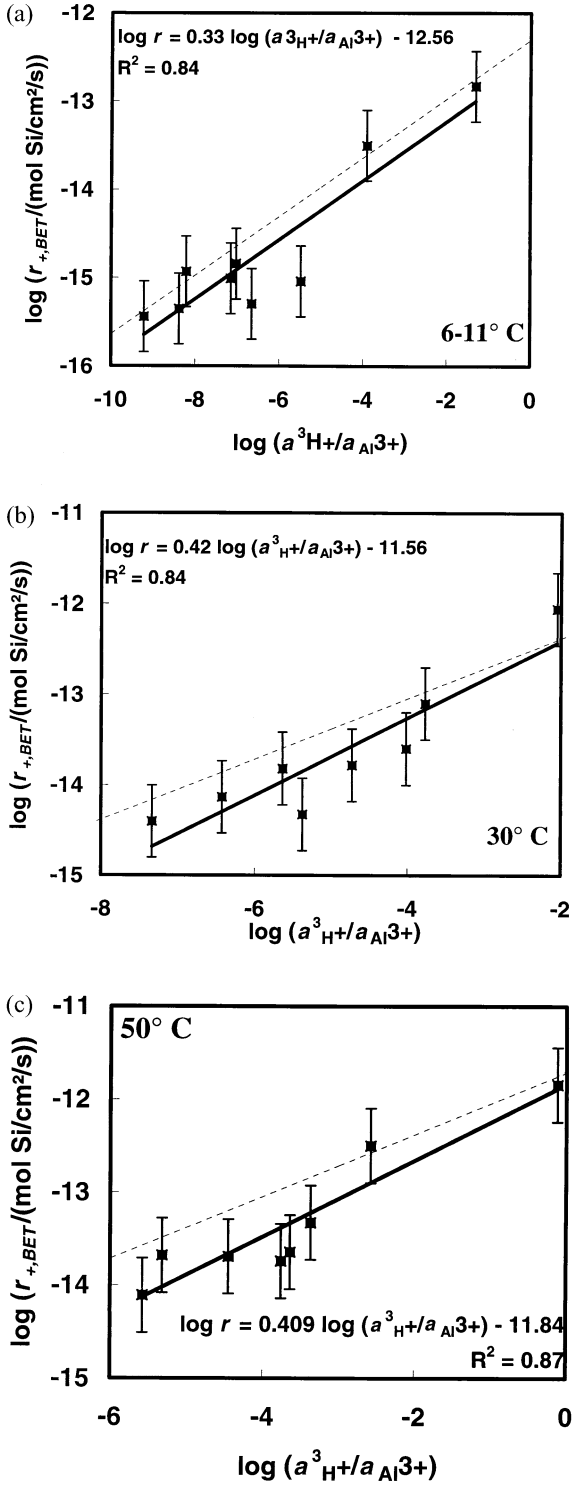

Fig. 6. Variation of the logarithm of $r_{+,BET}$ obtained in the present study at temperatures of ~9°, ~30°, and ~50°C with log $(a^3_{H^+}/a_{Al^{3+}})$. The filled squares correspond to experimental data reported in Table 4 and the error bars correspond to a ±0.4 log unit uncertainty (see text). The solid line represents a least squares fit of the data; the equation and coefficient of determination (R^2) of this line are given in the figure. The dashed curve corresponds to the results of a global fit of basaltic glass dissolution rate data at temperatures from 6 to 300°C, as generated using Eqn. 13 together with values of $10^{-5.6}$ (mol of Si)/cm^2/s and 25.5 kJ/mol, respectively for A_A and E_A, and a surface roughness of 92.

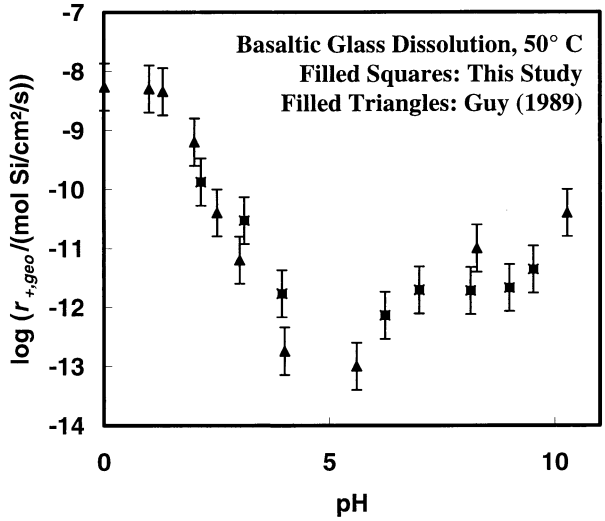

Fig. 7. Variation of measured geometric surface area normalized basaltic glass dissolution rates at 50°C as a function of pH.

is not the case for other basaltic glass dissolution rate data available in the literature. As can be seen by the close comparison between all the symbols and the line in Figure 8, Eqn. 13 provides a good description of the experimental data. The average difference between the logarithms of computed and measured dissolution rates is 0.34 log units. This difference exceeded 0.5 log units for 22% of the experimental data points. Note that this comparison includes basaltic glass dissolution rate data obtained at temperatures from 6 to 300°C, at pH from

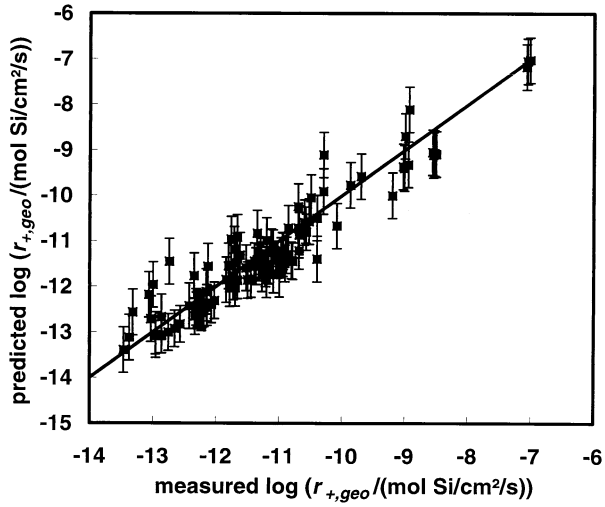

Fig. 8. Computed $r_{+,geo}$ as a function of their experimental counterparts. The solid squares correspond to basaltic glass dissolution rates, whereas the solid line corresponds to equal rates. Computed rates were generated using Eqn. 13 together with values of $10^{-5.6}$ (mol of Si)/cm^2/s and 25.5 kJ/mol, respectively for A_A and E_A, and aqueous activity ratios computed using the EQ3 computer code (Wolery, 1983). Experimental data used in this comparison were taken from this study as well as from Guy (1989), Berger et al. (1994b), Daux et al. (1997), and Oelkers and Gislason (2001) and cover a temperature range from 6 to 300°C and pH from 1 to 11 (see text and Appendix).

1 to 11, in reactive fluids containing varying concentrations of aqueous Si, Al, and oxalic acid, experiments performed in various reactor designs and laboratories. The close correspondence between computed and measured dissolution rates, therefore, supports strongly application of Eqn. 13 to describe basaltic glass dissolution rates. Furthermore, the close agreement between computed and measured rates illustrated in Figure 8 and tabulated in the Appendix support the likelihood that basaltic glass dissolution rates are controlled by the single mechanism described above over the full range of temperature, pH, and solution composition considered in these studies. Note that $r_{+,BET}$ values consistent with those measured in the present study can be obtained from Eqn. 13, $A_A = 10^{-5.6}$ (mol of Si)/cm(geo)^2/s and E_A = 25.5 kJ/mol, by dividing resulting $r_{+,geo}$ values by 92.

An equation describing basaltic glass dissolution rates over the full range of chemical affinity, aqueous solution composition and temperature can be generated from combining Eqns. 2 and 12 to obtain

$$\frac{r}{s} = A_A \exp\left(\frac{-E_A}{RT}\right)\left(\left(\frac{a^3_{H^+}}{a_{Al^{3-}}}\right)\Big/\left(1 + K_4\left(\frac{a^3_{H^+}}{a_{Al^{3+}}}\right)\right)\right)^{1/3} (1 - \exp(-A^*/\sigma RT). \quad (14)$$

The application of this equation, however, is currently limited owing to lack of detailed knowledge of σ and K_4 as a function of temperature, and A^* as a function of both aqueous solution composition and temperature. Insight into the value of σ and A^* is provided by Daux et al. (1997), who reported basaltic glass dissolution rates as a function of the chemical affinity of the hydrated basaltic glass surface layer at 90°C. Daux et al. (1997) noted that their basaltic glass dissolution rates were accurately described using Eqn. 2 where $\sigma = 1$ and A^* refers to the chemical affinity of the hydrated basaltic glass surface layer. This observation suggests that both $r \approx r_+$ and Eqn. 12 are applicable in all solutions for which $A^*/RT > 2.3$. Insight into the value of K_4 can be obtained by recalling that all data considered in the present study were found to be consistent with Eqn. 13. Because this equation is valid only if $K_4(a^3_{H^+}/a_{Al^{3+}})$ is substantially less than 1, a upper possible limit of K_4 can be estimated from the log $(a^3_{H^+}/a_{Al^{3+}})$ values listed in the Appendix. Consideration of these values suggests that log K_4 is less than 1 at 25°C and less than -3 at 300°C. Nevertheless, considering the wide range of solution compositions of the experiments in the Appendix, it seems likely that $K_4(a^3_{H^+}/a_{Al^{3+}})$ is substantially less than 1, and therefore Eqn. 13 will provide an accurate far-from-equilibrium basaltic glass dissolution rate estimates at most experimental and natural conditions.

The Arrhenius parameters, A_A and E_A generated in the present study are based on the assumption that basaltic glass dissolution rates are controlled by the destruction of partially detached Si tetrehedra formed by reaction 4. As such they describe the temperature variation of a rate constant that is the product of the far-from-equilibrium dissolution rate and the activity ratio $(a^3_{H^+}/a_{Al^{3+}})$. This differs from other applications of the Arrhenius equation in the geochemistry literature. For example, it has often been assumed that aluminosilicate dissolution is controlled by an activated complex formed through the adsorption of protons to the mineral surface (e.g., Hellmann, 1994; Blum and Stillings, 1995). Proton adsorption enhanced dissolution models yield rate constants that are proportional to the product $r_+ a^n_{H^+}$, where n refers to a reaction order. The difference in the Arrhenius parameters, A_A and E_A obtained in the present study and those generated assuming a proton adsorption enhanced dissolution model stems from the temperature variation of the aqueous activity of Al^{3+}. The activity of aqueous Al^{3+} varies dramatically with increasing temperature due to the variable relative stability of aqueous aluminum bearing species including Al^{3+}, $Al(OH)^{2+}$, $Al(OH)_2{}^+$, $Al(OH)_3$, and $Al(OH)_4{}^-$. Significant differences are, therefore, to be expected between A_A and E_A obtained in the present study and those reported in the literature based on other proposed dissolution mechanisms.

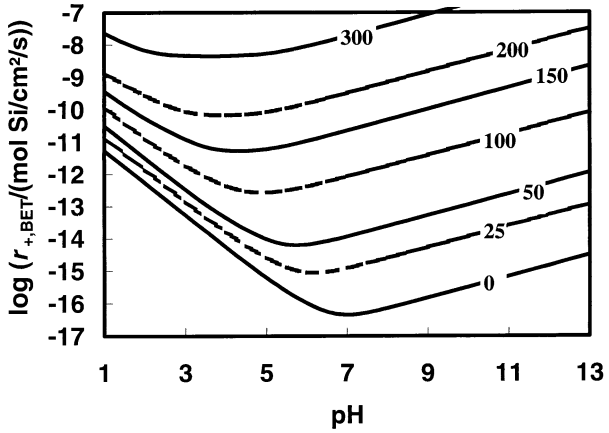

Fig. 9. Predicted $r_{+,BET}$ at temperatures from 0° to 300°C as a function of pH. Rates correspond to aqueous solutions having an ionic strength of 0.1 mol/kg, a total aqueous aluminum concentration of 10^{-6} mol/kg, and free of aluminum complexing aqueous species other than OH^-. All rates were computed using Eqn. 13 together with values of $10^{-5.6}$ (mol of Si)/cm^2/s, and 25.5 kJ/mol, respectively for A_A and E_A, a surface roughness of 92, and aqueous activity ratios computed using the EQ3 computer code (Wolery, 1983).

Computed values of $r_{+,BET}$ in 0.1 molal ionic strength solutions containing 10^{-6} mol/kg Al and void of Al complexing aqueous species other than OH^- are illustrated as a function of pH at various temperatures in Figure 9 and are tabulated in Table 5. This figure and table were created in terms of BET normalized surface areas to allow their comparison with BET surface area normalized dissolution rates of other minerals available in the literature. To be consistent with rates measured in the present study, $r_{+,BET}$ values shown in Figure 9 and listed in Table 5 were generated by dividing geometric surface area normalized rates generated from Eqn. 13 and the parameters listed above by 92, the surface roughness. It is noteworthy that far-from-equilibrium basaltic glass dissolution rates at near neutral conditions and $5 < pH < 9$ and temperatures from 0 to 30°C range from 10^{-16} to 10^{-14} mol/cm(BET)^2/s. These values are not significantly larger than corresponding values for enstatite (Oelkers and Schott, 2001), forsterite (Pokrovsky and Schott, 2000), or intermediate feldspars (see Blum and Stillings, 1995).

Table 5. Logarithms of computed $r_{+,BET}$ consistent with rates measured in the present study, as a function of temperature from 0 to 300° C and pH from 1 to 12.[a]

	log (r_{+BET}/(mol Si/cm^2/s)						
	Temperature						
pH	0	25	50	100	150	200	300
1	−11.22	−10.80	−10.45	−9.84	−9.43	−8.82	−7.59
1.5	−11.72	−11.30	−10.95	−10.33	−9.87	−9.18	−7.89
2	−12.22	−11.80	−11.45	−10.76	−10.21	−9.51	−8.12
2.5	−12.72	−12.30	−11.95	−11.21	−10.56	−9.80	−8.24
3	−13.22	−12.80	−12.45	−11.60	−10.87	−10.01	−8.28
3.5	−13.72	−13.18	−12.89	−11.95	−11.10	−10.10	−8.29
4	−14.21	−13.75	−13.31	−12.23	−11.21	−10.12	−8.29
4.5	−14.70	−14.17	−13.67	−12.40	−11.22	−10.09	−8.27
5	−15.16	−14.54	−13.96	−12.43	−11.16	−10.02	−8.22
5.5	−15.58	−14.84	−14.13	−12.37	−11.06	−9.91	−8.13
6	−15.94	−14.99	−14.13	−12.25	−10.92	−9.76	−7.99
6.5	−16.21	−14.97	−14.03	−12.10	−10.76	−9.60	−7.84
7	−16.30	−14.86	−13.88	−11.94	−10.60	−9.44	−7.68
7.5	−16.23	−14.71	−13.72	−11.78	−10.43	−9.27	−7.51
8	−16.10	−14.55	−13.56	−11.61	−10.27	−9.10	−7.34
8.5	−15.94	−14.38	−13.39	−11.44	−10.10	−8.94	−7.18
9	−15.78	−14.22	−13.23	−11.28	−9.94	−8.77	−7.01
9.5	−15.61	−14.05	−13.06	−11.11	−9.77	−8.61	−6.85
10	−15.44	−13.88	−12.89	−11.02	−9.60	−8.44	−6.68
10.5	−15.28	−13.72	−12.73	−10.86	−9.44	−8.27	−6.51
11	−15.11	−13.55	−12.56	−10.69	−9.27	−8.11	−6.35
11.5	−14.94	−13.38	−12.40	−10.53	−9.10	−7.94	−6.18
12	−14.78	−13.22	−12.23	−10.36	−8.93	−7.77	−6.01

[a] Rates in this table correspond to aqueous solutions having an ionic strength of 0.1 mol/kg, a total aqucous aluminum concentration of 10^{-6} mol/kg, and free of aluminum complexing aqeous species other than OH^-. All rates were computed using Eqn. 13 together with values of $10^{-5.6}$ (mol of Si)/cm^2/s, and 25.5 kJ/mol, respectively, for $A°_A$ and $E°_A$, a surface roughness of 92, and aqueous activity ratios computed using the EQ3 computer code (Wolery, 1983). To generate $r_{+,geo}$ multiply r_{+BET} provided in this table by the surface roughness of 92.

5. EXPERIMENTAL AND COMPUTATIONAL UNCERTAINTIES

Uncertainties associated with the rate constants generated in this study arise from a variety of sources, including the measurement of aqueous solution concentrations, fluid flow rates, and glass surface areas. The uncertainties in the measured values of the total aqueous silica and aluminum concentration are on the order of ±10% or less, except for the few calorimetric Si analyses that may have had higher uncertainties due to Fe interference. Computational and experimental uncertainties in the pH of these solutions are on the order of ±0.1 pH units. Uncertainties in fluid flow rate measurements are not more than 4%. In contrast, uncertainties associated with the measurement of the surface area of the initial basaltic glass powder are ±10%. If uncertainties were estimated exclusively from the sum of these contributions, an overall uncertainty of the initial BET surface area normalized dissolution rates listed in Table 4 would be on the order of 20%. Although this estimate appears to be consistent with the rates obtained from a single steady state (cf. Figs. 2 and 3), it is substantially less than the apparent scatter among the rates obtained from different steady-state conditions as depicted in Figure 5. This discrepancy possibly stems from an evolution of basaltic glass reactive surface area during the course of the experiments. Values listed in Table 1 indicate that basaltic glass BET surface area evolved significantly during the dissolution experiments performed in this study. As emphasized by Gautier et al. (2001), the degree to which reactive surface area varies in response to BET surface area changes is currently impossible to define unambiguously. Consequently, overall uncertainties associated with the rates reported in the present study are unclear. Consideration of the scatter in the Figure 6, and comparison of geometrical surface area normalized rates obtained in the present study with those reported by Guy (1989), however, suggests that the overall uncertainty on the basaltic glass dissolution rates measured in the present study to be on the order of ±0.4 log units.

6. CONCLUSIONS

Basaltic glass far-from-equilibrium dissolution rates are found to be consistent with $r_+ \alpha (a^3_{H^+}/a_{Al^{3+}})^{1/3}$ over the pH range 2–11 at temperatures from 6 to 50°C. This observation suggests that basaltic glass dissolution is controlled by a single mechanism over this pH and temperature range. This observation confirms over a larger temperature and pH range the basaltic glass dissolution mechanism proposed by Oelkers and Gislason (2001) consisting of 1) the relatively rapid and essentially complete removal of univalent and divalent cations from the near surface, 2) aluminum releasing exchange reactions between three aqueous H^+ and Al in the basaltic glass structure, followed by 3) the relatively slow detachment of silica from partially liberated glass network.

Geometric surface area normalized basaltic glass dissolution

rates obtained in this study were found to be consistent, within uncertainty, of those reported by Guy (1989). This consistency allowed simultaneous regression of basaltic glass dissolution rate data obtained from Guy (1989), Berger et al. (1994b), Daux et al. (1997), Oelkers and Gislason (2001), and the present study to a single transition state rate equation containing only two regression parameters, an Arrhenius activation energy and a preexponential term. This rate equation allows description, within uncertainty, of over 100 independently measured dissolution rates obtained at pH ranging from 1 to 11, temperatures from 6 to 300°C, and in solutions enriched in aqueous Al, Si and organic acids. Owing to the success of this rate equation to describe laboratory measured rates, it seems likely that it can be used with equal success to describe these basaltic glass dissolution rates in natural systems, as long as their surface areas can be accurately characterized. The relative release rates of metals from basaltic glass during its dissolution at a variety of pH, and the application to natural systems of basaltic glass dissolution rates generated using equations reported and parameterized in the present study will be the focus of further manuscript in this series.

Acknowledgments—Matthildur B. Stefńsdóttir, Eydís S. Eiríksdóttir, Audur Andrésdóttir, Andri Stefńsson, Ingvi Gunnarsson, Björn Gudmundsson, Domenik Wolff-Boenisch, Jacques Schott, Stephan Kohler, and Oleg Pokrovsky assisted in many ways during the course of this work. Don Voight at Penn State University measured the surface area of the glasses. An early version of this paper benefited from critical reviews by two anonymous reviewers and the associate editor Enrique Merino. We are grateful for all of their help and assistance. The first draft of this manuscript was written at the 12th to 15th century castle at Castet d'Aleu located in the south of France while our families played in the garden and/or prepared lunch. We thank them for their understanding and patience. This research was supported by the Icelandic Science Foundation 962290098, the Research Fund of the University of Iceland, the Centre National de la Recherche Scientifique and the European Commission through the TMR program (contract HPRN-CT-2000-00058).

Associate editor: E. Merino

REFERENCES

Aagaard P. and Helgeson H. C. (1977) Thermodynamic and kinetic constraints on the dissolution of feldspars. *Geol. Soc. Am. Abstr.* **9,** 873.

Aagaard P. and Helgeson H. C. (1982) Thermodynamic and kinetic constraints on reaction rates among minerals and aqueous solutions: I. Theoretical considerations. *Am. J. Sci.* **282,** 237–285.

Alt J. C., Honnores J., Laverne C., and Emmermann R. (1986) Hydrothermal alteration of a 1 km section through the upper oceanic crust. Deep Sea Drilling Project Hole 504B: Mineralogy, chemistry, and evolution of seawater-basalt interactions. *J. Geophys. Res.* **91,** 10309–10335.

Banfield J. F., Jones B. F., and Veblen D. R. (1991) An AEM-TEM study of weathering and diagenesis, Abert Lake, Oregon: I. Weathering reactions in the volcanics. *Geochim. Cosmochim. Acta* **55,** 2781–2793.

Berger G., Schott J., and Loubet M. (1987) Fundamental processes controlling the first stage of alteration of a basaltic glass by seawater: An experimental study between 200 and 320°C. *Earth Planet. Sci. Lett.* **84,** 431–445.

Berger G., Schott J., and Guy C. (1988) Behaviour of Li, Rb, and Cs during basalt glass and olivine dissolution and chlorites, smectites and zeolites precipitation from seawater: Experimental investigation and modelization between 50°C and 300°C. *Chem. Geol.* **71,** 297–312.

Berger G., Cadore E., Schott J., and Dove P. (1994a) Dissolution rate of quartz in Pb and Na electrolyte solutions. Effect of the nature of the surface complexes and reaction affinity. *Geochim. Cosmochim. Acta* **58,** 541–551.

Berger G., Clarapols C., Guy C., and Daux V. (1994b) Dissolution rate of basaltic glass in silica-rich solutions: Implications for long term alteration. *Geochim. Cosmochim. Acta* **58,** 4875–4886.

Berger G., Beaufort D., and Lacharpagne J.-C. (2002) Experimental dissolution of sanadine under hydrothermal conditions: Mechanism and rate. *Am. J. Sci.* **301,** 663–685.

Berner R. A. (1992) Weathering, plants, and the long-term carbon cycle. *Geochim. Cosmochim. Acta* **56,** 3225–3231.

Berner E. K. and Berner R. A. (1996) *Global Environment: Water, Air, and Geochemical Cycles.*Prentice-Hall.

Bourcier W. L., Peiffer D. W., Knauss K. G., McKeegan K., and Smith D. K. (1989) A kinetic model for borosilicate glass dissolution based on the dissolution affinity of a surface altered layer. In *Scientific Basis for Nuclear Waste Management XIII* (eds. V. M. Oversby and P. W. Brown), pp. 120–128. Mat. Res. Soc.

Blum A. E. and Stillings L. L. (1995) Feldspar dissolution kinetics. *Rev. Mineral.* **31,** 291–351.

Brady P. V. and Gislason S. R. (1997) Seafloor weathering controls on atmospheric CO_2 and global climate. *Geochim. Cosmochim. Acta* **61,** 965–973.

Casey W. H., Westrich H. R., Massis T., Banfield J. F., and Arnold G. W. (1989) The surface chemistry of labradorite feldspar after acid hydrolysis. *Chem. Geol.* **78,** 205–218.

Chester R. (2000) *Marine Geochemistry.*2nd ed. Blackwell Science.

Colman S. M. (1982) *Chemical Weathering of Basalts and Andesites.* Professional Paper 1246. U.S. Geological Survey.

Crovisier J. L. (1989) Dissolution des verres basaltiques dans l'eaude mer et dans l'eau douce Essai de modélisation. Ph.D. dissertation. L'Université Louis Pasteur.

Crovisier J. L, Fritz B., Grambow B., and Eberhart J. P. (1985) Dissolution of basaltic glass: Experiments and thermodynamic modelling. In *Scientific Basis for Nuclear Waste Management,*Vol. 50 (ed. L. Werme), pp. 273–280. Materials Research Society.

Crovisier J. L., Honnorez J., and Eberhart J. P. (1987) Dissolution of basaltic glass in seawater: Mechanism and rate. *Geochim. Cosmochim. Acta* **51,** 2977–2990.

Daux V., Guy C., Advocat T., Crovisier J., and Stille M. (1997) Kinetic Aspects of basaltic glass dissolution at 90°C: Role of silicon and aluminum. *Chem. Geol.* **142,** 109–128.

Dessert C., Dupre B., Francois L. M., Schott J., Gaillardet J., Chakarapani G., and Bajpai S. (2001) Erosion of. Deccan traps determined by river geochemistry: Impact on the global climate and the $^{87}Sr/^{86}Sr$ ratio of seawater. *Earth Planet. Sci. Lett.* **188,** 459–474.

Dove P. M. and Crerar D. A. (1990) Kinetics of quartz dissolution in electrolyte solutions using a hydrothermal mixed flow reactor. *Geochim. Cosmochim. Acta* **54,** 955–969.

Eggleton R. A., Foudoulis C., and Farkevisser D. (1987) Weathering of basalt: Changes in rock chemistry and mineralogy. *Clays Clay Minerals* **35,** 161–169.

Fishman M. J. and Friedman L. C., eds. (1989) Method for determination of inorganic substances in water and fluvial sediments. In *Techniques of Water-Resources Investigations of the United States Geological Survey,*Book 5, *Laboratory Analysis.*U.S. Department of the Interior.

Francois L. M. and Walker J. C. G. (1992) Modeling the phanerozoic carbon cycle and climate: Constraints from the $^{87}Sr/^{86}Sr$ isotopic ratio of seawater. *Am. J. Sci.* **292,** 81–135.

Furnes H. (1975) Experimental plagonitization of basaltic glasses of varied composition. *Contrib. Mineral. Petrol.* **50,** 103–113.

Gautier J.-M., Oelkers E. H., and Schott J. (2001) Are quartz dissolution rates proportional to BET surface areas? *Geochim. Cosmochim. Acta* **65,** 1059–1070.

GERM (2000) The geochemical earth reference model. Available at: http://EarthRef.org.

Gislason S. R. and Eugster H. P. (1987) Meteoric water-basalt interactions: I. A laboratory study. *Geochim. Cosmochim. Acta* **51,** 2827–2840.

Gislason S. R. and Arnórsson S. (1990) Saturation state of natural waters in Iceland relative to primary and secondary minerals in basalts. In *Fluid–Mineral Interactions: A Tribute to H. P. Eugster* (eds. R. J. Spencer and I.-M. Chou), pp. 373–393. Special Publication 2. Geochemical Society.

Gislason S. R., Andrésdóttir A., Sveinbjörnsdóttir A. E., Óskarsson N., Thordarson Th., Torssander P., Novâk N., and Zâk K. (1992) Local effects of volcanoes on the hydrosphere: Example from Hekla, southern Iceland. In *Water–Rock Interactions* (eds. Y. K. Kharaka and A. S. Maest), pp. 477–481. Balkema.

Gislason S. R. and Arnórsson S. (1993) Dissolution of primary basaltic minerals in natural waters: Saturation state and kinetics. *Chem. Geol.* **105,** 117–135.

Gislason S. R., Veblen D. R., and Livi K. J. T. (1993) Experimental meteoric water-basalt interactions: Characterization and interpretation of alteration products. *Geochim. Cosmochim. Acta* **57,** 1459–1471.

Gislason S. R., Arnórsson S., and Ármannsson H. (1996) Chemical weathering of basalt in SW Iceland: Effects of runoff, age of rocks and vegetative/glacial cover. *Am. J. Sci.* **296,** 837–907.

Grambow B. (1985) A general rate equation for nuclear waste glass corrosion. *Mat. Res. Soc. Symp. Proc.* **44,** 15–27.

Gratz A. J., Manne S., and Hansma P. (1991) Atomic Force Microscopy of atomic-scale ledges and etch pits formed during dissolution of quartz. *Science* **251,** 1343–1346.

Gratz A. J. and Bird P. (1993) Quartz dissolution: Negative crystal experiments and a rate law. *Geochim. Cosmochim. Acta* **57,** 965–976.

Guy C. (1989) Méchanimes de dissolution des solides dans les solutions hydrothermales déduits du comportement des verres basaltiques et de calcites déformées. Ph.D. thesis. Université Paul Sabatier.

Guy C. and Schott J. (1989) Multisite surface reaction versus transport control during hydrolysis of a complex oxide. *Chem. Geol.* **78,** 181–204.

Helgeson H. C., Murphy W. M., and Aagaard P. (1984) Thermodynamic and kinetic constraints on reaction rates among minerals and aqueous solutions: II. Rate constants, effective surface area, and the hydrolysis of feldspar. *Geochim. Cosmochim. Acta* **48,** 2405–2432.

Hellmann R. (1994) The albite–water system: Part I. The kinetics of dissolution as a function of pH at 100, 200, and 300°C. *Geochim. Cosmochim. Acta* **58,** 595–611.

Holland H. D. (1978) *The Chemistry of the Atmosphere and Oceans.* Wiley.

Hoppe H. (1940) Untersuchungen an Palagonittuffen und ihre Bildungsbedingungen. *Chem. Erde* **13,** 484–514.

Humpris S. E. and Thompson G. (1978) Hydrothermal alteration of ocean basalts by seawater. *Geochim. Cosmochim. Acta* **42,** 107–125.

Johnson J. W., Oelkers E. H., and Helgeson H. C. (1992) SUPCRT92: A software package for calculating the standard molal properties of minerals gases, aqueous species and reactions among them from 1 to 5000 bars and 0 to 1000°C. *Comp. Geosci.* **18,** 899–947.

Kristmannsdóttir H. (1982) Alteration in the IRDP drill hole compared with other drill holes in Iceland. *J. Geophys. Res.* **87,** 6525–6531.

Kristmannsdóttir H. and Tómasson J. (1978) Zeolite zones in geothermal areas in Iceland. In *Natural Zeolites, Occurrences, Properties, Use* (eds. L. Sand and F. Mumpton), pp. 277–284. Pergamon.

Kump L. R., Brantley S. L., and Authur M. A. (2000) Chemical weathering, atmospheric CO_2, and climate. *Annu. Rev. Earth Planet. Sci.* **28,** 611–667.

Lasaga A. C. (1981) Transition state theory. *Rev. Mineral.* **8,** 135–169.

Lasaga A. C., Soler J. M., Ganor J., Burch T. E., and Nagy K. L. (1994) Chemical weathering rate laws and global geochemical cycles. *Geochim. Cosmochim. Acta* **58,** 2362–2386.

Louvat P. (1997) Étude géochimique de l'érosion fluviale dîles volcaniques a l'aide des bilans d'éléments majeurs et traces. Ph.D. thesis. University of Paris.

McDuff R. E. and Morel F. M. M. (1980) The geochemical control of seawater (Sillen revisited). *Environ. Sci. Technol.* **14,** 1182–1186.

Metz V. and Ganor J. (2001) Stirring effect on kaolinite dissolution rate. *Geochim. Cosmochim. Acta* **65,** 3475–3490.

Moulton K. L., West J., and Berner R. A. (2000) Solute flux and mineral mass balance approaches to the quantification of plant effects on silicate weathering. *Am. J. Sci.* **300,** 539–570.

Murphy W. M. and Helgeson H. C. (1987) Thermodynamic and kinetic constraints on reaction rates among minerals and aqueous solutions. III. Activated complexes and the pH-dependence of the rates of feldspar, pyroxene, wollastonite, and olivine hydrolysis. *Geochim. Cosmochim. Acta* **51,** 3137–3153.

Murphy W. M., Oelkers E. H., and Lichtner P. C. (1989) Surface reaction versus diffusion control of mineral dissolution and growth rates in geochemical processes. *Chem. Geol.* **78,** 357–380.

Nesbitt H. W. and Wilson R. E. (1992) Recent chemical weathering of basalts. *Am. J. Sci.* **292,** 740–777.

Oelkers E. H. (2001) A general kinetic description of multi-oxide silicate mineral and glass dissolution. *Geochim. Cosmochim. Acta* **65,** 3703–3719.

Oelkers E. H., Schott J., and Devidal J.-L. (1994) The effect of aluminum, pH, and chemical affinity on the rates of aluminosilicate dissolution reactions. *Geochim. Cosmochim. Acta* **58,** 2011–2024.

Oelkers E. H. and Schott J. (1995) Experimental study of anorthite dissolution and the relative mechanism of feldspar hydrolysis. *Geochim. Cosmochim. Acta* **59,** 5039–5053.

Oelkers E. H., Gislason S. R., and Schott J. (1999) A general mechanism for multi-oxide solid dissolution and its application to basaltic glass. In *Geochemistry of the Earth's Surface* (ed. H. Ármannsson), pp. 413–416. Balkema.

Oelkers E. H. and Schott J. (1999) An experimental study of the dissolution rate of kyanite as a function of chemical affinity and solution composition. *Geochim. Cosmochim. Acta* **63,** 785–798.

Oelkers E. H. and Gislason S. R. (2001) The mechanism, rates, and consequences of basaltic glass dissolution: I. An experimental study of the dissolution rates of basaltic glass as a function of aqueous Al, Si, and oxalic acid concentration at 25°C and pH = 3 and 11. *Geochim. Cosmochim. Acta* **65,** 3671–3681.

Oelkers E. H. and Schott J. (2001) An experimental study of enstatite dissolution rates as a function of pH, temperature, and aqueous Mg and Si concentration, and the mechanism of pyronene/pyroxenoid dissolution. *Geochim. Cosmochim. Acta* **65,** 1219–1231.

Pokrovskii V. A. and Helgeson H. C. (1995) Thermodynamic properties of aqueous species and the solubilities of minerals at high pressures and temperatures: The system Al_2O_3-H_2O-NaCl. *Am. J. Sci.* **295,** 1255–1342.

Pokrovsky O. and Schott J. (2000) Kinetics and mechanism of forsterite dissolution at 25°C and pH from 1 to 12. *Geochim. Cosmochim. Acta* **64,** 3313–3326.

Ronov A. B. and Yaroshevsky A. A. (1976) A new model for the chemical structure of the Earth's crust. *Geochem. Int.* **13,** 89–121.

Riley J. P. and Chester R. (1971) *Introduction to Marine Chemistry.* Academic Press.

Schott J. and Oelkers E. H. (1995) Dissolution and crystallization rates of silicate minerals as a function of chemical affinity. *Pure Appl. Chem.* **67,** 603–610.

Seyfried W. E. Jr. and Bischoff J. L. (1979) Low temperature basalt alteration by seawater: An experimental study at 70°C and 150°C. *Geochim. Cosmochim. Acta* **43,** 1937–1947.

Sigurdsson F. and Ingimarsson J. (1990) The hydraulic conductivity of Icelandic rocks (in Icelandic). In *Water and the Country* (ed. G. Sigbjarnarson), pp. 121–128. National Energy Authority, Reykjavik.

Spivack A. J. and Staudigel H. (1994) Low-temperature alteration of the upper oceanic crust and the alkalinity budget of seawater. *Chem. Geol.* **115,** 239–247.

Staudigel H., Hart S. R., Schmincke H., and Smith B. M. (1989) Cretaceous ocean crust at DSDP site-4417 and site-418: Carbon uptake from weathering versus loss by magmatic outgassing. *Geochim. Cosmochim. Acta* **53,** 3091–3094.

Stefánsson A. and Gislason S. R. (2001) Chemical weathering of basalts, SW Iceland: Effect of rock crystallinity and secondary minerals on chemical fluxes to the ocean. *Am. J. Sci.* **301,** 513–556.

Teng H. and Grandstaff D. E (1995) Dissolution of basaltic glass: Effects of pH and organic ligands. In *Scientific Basis for Nuclear Waste Management V. XIX,*Vol. 412 (eds. W. M. Murphy and D. A. Knecht), pp. 249–256. Materials Research Society.

Thomassin J. H., Boutonnat F., Touray J. C., and Baillif P. (1989) Geochemical role of the water/rock ratio during the experimental alteration of synthetic basaltic glass at 50°C: An XPS and STEM investigation. *Eur. J. Mineral.* **1,** 261–274.

Thompson G. (1983) Basalt–seawater interaction. In *Hydrothermal Processes at Seafloor Spreading Centers* (eds. P. A. Rona, K. Bostom, L. Laubier, and K. L. Smith), pp. 225–278. Plenum.

Thorseth I. H., Furnes H., and Tumyr O. (1995) Textural and chemi-

caleffects of bacterial activity on basaltic glass: An experimental approach. *Chem. Geol.* **119,** 139–160.
Urey H. C. (1952) *The Planets, Their Origin and Development.*Yale University Press.
Wang Z. Y., Wang Y., and Merino E. (1995) Dynamic weathering model: Constraints required by coupled dissolution and pseudomorphic replacement. *Geochim. Cosmochim. Acta* **59,** 1559–1570.
Wolery T. J. (1983) *EQ3NR, a Computer Program for Geochemical Aqueous Speciation-Solubility Calculations: User's Guide and Documentation.*UCRL-53414. Lawrence Livermore National Laboratory.
Wolff-Boenisch D., Gislason S. R., and Oelkers E. H. (2002) Dissolution rates of volcanic glasses of different chemical compositions (abstract). *Geochim. Cosmochim. Acta* **66,** A843.

Appendix. Comparison of experimentally measured and computed log $r_{+,geo}$. Computed rates were generated using Eqn. 13 together with values of $10^{-5.6}$ (mol of Si)/cm^2/s, and 25.5 kJ/mol, respectively, for A_A and E_A.

Reference	T, °C	In situ pH	log $\left(a^3_{H^+}/a_{Al^{3+}}\right)$[a]	log $r_{+,geo}$ (expt.)	log $r_{+,geo}$ (cal.)	Δ log $r_{+,geo}$[b]
This study						
	6	4.37	−5.49	−13.07	−12.18	0.89
	6	4.86	−6.66	−13.33	−12.56	0.77
	7	7.08	−9.22	−13.48	−13.39	0.09
	7	8.25	−8.39	−13.38	−13.12	0.26
	7	9.49	−8.22	−12.97	−13.06	−0.11
	7	10.31	−7.16	−13.04	−12.71	0.33
	7	11.11	−7.03	−12.88	−12.77	−0.11
	10	3.34	−3.91	−11.54	−11.59	−0.05
	11	2.25	−1.31	−10.87	−10.71	0.16
	30	4.17	−5.38	−12.36	−11.76	0.60
	30	3.31	−3.77	−11.14	−11.23	−0.09
	30	2.40	−2.05	−10.09	−10.66	−0.57
	29	6.75	−7.34	−12.44	−12.42	0.02
	30	7.94	−6.43	−12.17	−12.11	0.06
	30	8.88	−5.64	−11.85	−11.85	0.00
	30	9.95	−4.73	−11.82	−11.55	0.27
	30	10.55	−4.02	−11.64	−11.31	0.33
	50	3.94	−3.76	−11.77	−10.96	0.81
	50	6.23	−5.58	−12.14	−11.56	0.58
	50	6.99	−5.32	−11.71	−11.47	0.24
	50	8.13	−4.45	−11.73	−11.18	0.54
	50	8.99	−3.64	−11.68	−10.92	0.76
	50	9.52	−3.37	−11.36	−10.83	0.53
	50	3.10	−2.58	−10.53	−10.57	−0.04
	49	2.14	−0.12	−9.88	−9.77	0.11
	30	5.31	−8.85	−12.59	−12.90	−0.31
	60	5.03	−7.65	−11.71	−12.11	−0.40
	100	4.80	−5.86	−11.20	−11.10	0.10
	149	4.58	−3.32	−10.55	−9.84	−0.79
Guy (1989)	50	2	−0.85	−9.20	−9.99	−0.79
	50	2.5	−2.35	−10.40	−10.49	−0.09
	50	3	−3.85	−11.20	−10.98	0.22
	50	4	−5.25	−12.74	−11.44	1.30
	50	5.6	−6.80	−13.00	−11.96	1.04
	50	8.27	−6.08	−11.00	−11.72	−0.72
	50	10.27	−5.08	−10.39	−11.39	−1.00
	100	2.51	−1.25	−9.70	−9.58	0.12
	100	3.01	−2.66	−10.50	−10.04	0.46
	100	4.01	−4.32	−10.60	−10.59	−0.04
	100	5.6	−4.70	−10.70	−10.71	−0.01
	100	7.24	−3.26	−10.70	−10.24	0.46
	100	9.24	−2.25	−10.30	−9.91	0.39
	200	4.04	−2.10	−8.90	−9.10	−0.20
	200	6.20	−0.85	−9.0	−8.96	0.04
	200	8.18	0.91	−8.5	−8.10	0.40
Oelkers and Gislason (2001)	25	3.05	−5.38	−11.20	−11.83	−0.63
	25	3.08	−3.99	−10.94	−11.38	−0.44
	25	3.01	−5.96	−11.70	−12.03	−0.33
	25	3.00	−3.79	−10.90	−11.31	−0.41
	25	3.04	−5.06	−11.09	−11.73	−0.64
	25	3.03	−3.52	−10.94	−11.23	−0.29
	25	3.09	−3.79	−10.89	−11.31	−0.42
	25	3.10	−2.24	−10.57	−10.80	−0.23

(continued)

Appendix A. (Continued)

Reference	*T*, °C	In situ pH	log $(a^3_{H^+}/a_{Al^{3+}})$[a]	log $r_{+,geo}$ (expt.)	log $r_{+,geo}$ (cal.)	Δ log $r_{+,geo}$[b]
Oelkers and Gislason (2001)	25	3.08	−4.12	−10.81	−11.42	−0.61
	25	3.08	−3.82	−10.97	−11.32	−0.35
	25	3.18	−3.49	−10.69	−11.21	−0.52
	25	3.03	−3.49	−10.95	−11.21	−0.27
	25	3.16	−1.77	−10.58	−10.64	−0.06
	25	3.00	−3.51	−10.94	−11.22	−0.28
	25	2.99	−4.42	−11.19	−11.52	−0.32
	25	2.96	−5.53	−11.73	−11.89	−0.16
	25	3.11	−5.97	−11.78	−12.03	−0.25
	25	3.03	−5.46	−11.66	−11.87	−0.20
	25	3.00	−4.19	−11.39	−11.45	−0.06
	25	2.98	−3.31	−11.10	−11.15	−0.05
	25	3.11	−4.29	−11.32	−11.47	−0.15
	25	3.04	−4.52	−11.37	−11.56	−0.19
	25	3.05	−4.09	−11.05	−11.41	−0.36
	25	3.03	−4.11	−11.03	−11.42	−0.39
	25	2.98	−4.66	−11.22	−11.60	−0.38
	25	3.00	−4.97	−11.27	−11.70	−0.43
	25	2.95	−5.36	−11.45	−11.83	−0.38
	25	2.97	−5.44	−11.50	−11.86	−0.36
	25	3.08	−4.49	−11.17	−11.55	−0.38
	25	2.98	−4.05	−11.02	−11.40	−0.38
	25	3.04	−3.85	−11.30	−11.33	−0.03
	25	3.00	−4.12	−11.28	−11.42	−0.13
	25	3.10	−4.45	−11.20	−11.53	−0.33
	25	2.91	−4.18	−10.79	−11.44	−0.65
	25	3.03	−4.33	−10.91	−11.49	−0.58
	25	10.97	−6.80	−12.03	−12.31	−0.28
	25	10.97	−6.96	−12.15	−12.36	−0.21
	25	10.96	−7.34	−12.29	−12.51	−0.22
	25	10.98	−7.06	−12.08	−12.39	−0.31
	25	10.98	−8.37	−12.57	−12.83	−0.26
	25	11.00	−7.33	−12.19	−12.48	−0.29
	25	10.92	−8.66	−12.66	−12.92	−0.26
	25	10.97	−7.60	−12.23	−12.57	−0.34
	25	11.01	−7.25	−12.15	−12.49	−0.31
	25	11.00	−7.37	−12.22	−12.50	−0.28
	25	11.03	−7.48	−12.31	−12.53	−0.22
	25	10.99	−7.47	−12.24	−12.53	−0.29
	25	11.00	−7.36	−12.30	−12.49	−0.29
	25	11.02	−7.46	−12.32	−12.53	−0.21
	25	11.00	−7.43	−12.26	−13.52	−0.26
	25	10.94	−8.91	−12.76	−13.00	−0.24
	25	11.06	−7.85	−12.34	−12.65	−0.31
	25	11.01	−9.15	−12.96	−13.08	−0.12
	25	10.99	−9.08	−12.86	−13.06	−0.20
	25	11.04	−7.24	−12.32	−12.45	−0.13
Berger et al. (1994)	150	2.0	−1.10	−8.54	−9.10	−0.56
	150	2.0	−1.05	−8.51	−9.08	−0.27
	150	2.0	−0.93	−8.56	−9.05	−0.49
	150	2.0	−0.99	−8.53	−9.07	−0.54
	150	2.0	−1.75	−8.95	−9.32	−0.37
	150	2.0	−1.98	−9.01	−9.39	−0.38
	150	2.0	−1.88	−9.03	−9.36	−0.33
	300	1.0	2.64	−7.06	−7.05	0.01
	300	1.0	2.26	−7.07	−7.17	−0.10
	300	1.0	2.71	−7.02	−7.02	0.00
Daux et al. (1997)	90	8.2	−4.42	−10.69	−10.71	−0.02
	90	8.2	−4.48	−10.69	−10.74	−0.05
	90	8.1	−4.86	−10.69	−10.86	−0.17

[a] The activity ratio listed in this table is that computed for the indicated experimental temperature.
[b] $\Delta \log r_{+,geo} = \log r_{+,geo}$ (cal.) − $\log r_{+,geo}$ (expt.).